THE JOURNAL OF PHYSICAL CHEMISTRY Letters

Letter

pubs.acs.org/JPCL

How the Reorganization Free Energy Affects the Reduction Potential of Structurally Homologous Cytochromes

Isabella Daidone,[†] Andrea Amadei,[‡] Francesco Zaccanti,[§] Marco Borsari,[§] and Carlo Augusto Bortolotti*[,∥,⊥]

[†]Department of Physical and Chemical Sciences, University of L'Aquila, via Vetoio (Coppito 1), 67010 L'Aquila, Italy

[‡]Department of Chemical Sciences and Technologies, University of Rome "Tor Vergata", via della Ricerca Scientifica 1, 00133 Rome, Italy

[§]Department of Chemical and Geological Sciences and [∥]Department of Life Sciences, University of Modena and Reggio Emilia, via Campi 183, 41125 Modena, Italy

[⊥]CNR-Nano Institute of Nanoscience, via Campi 213/A, 41125 Modena, Italy

Supporting Information

ABSTRACT: Differences in the reduction potential E^0 among structurally similar metalloproteins cannot always be fully explained on the basis of their 3-D structures. We investigate the molecular determinants to E^0 using the mixed quantum mechanics/molecular mechanics approach named perturbed matrix method (PMM); after comparison with experimental values to assess the reliability of our calculations, we investigate the relationship between the change in free energy upon reduction ΔA^0 and the reorganization energy. We find that the reduction potential of cytochromes can be regarded as the result of the sum of two terms, one being mostly dependent on the energy fluctuations within a limited range around the mean transition energy and the second being mostly dependent linearly on the difference $\Delta\lambda = \lambda_{red} - \lambda_{ox}$ of the reorganization free energies for the ox → red (λ_{red}) and for the red → ox (λ_{ox}) relaxations.

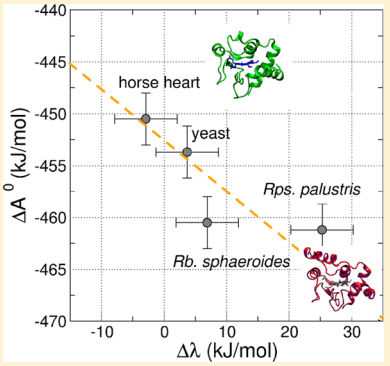

SECTION: Biophysical Chemistry and Biomolecules

Cytochromes are heme-containing proteins that serve as electron carriers in electron transfer (ET) chains and are ubiquitous in prokaryotes and eukaryotes.[1,2] Depending on the organism in which they operate and subsequently on their specific physiological role, cytochromes can be soluble or membrane-bound, displaying diverse folding, heme coordination, and physicochemical properties. In particular, their reduction potential E^0 can vary dramatically, spanning a 800 mV range.[3−5] Even cytochrome families with minor structural differences, such as mitochondrial cytochromes *c* (cyt*c* hereafter) and their nearest bacterial homologues, cytochromes c_2 (cytc_2), display important shifts in the reduction potential. In fact, mitochondrial cytochromes feature E^0 values that are close to +260 mV versus SHE (standard hydrogen electrode) in nearly all species, while E^0 of cytc_2 are generally around 100 mV more positive than those of cyt*c*, and in some cases they can be as high as +470 mV.[6]

Both cyt*c* and cytc_2 act as electron carriers between membrane-bound proteins, although in amazingly diverse organisms. (See Figure 1.) Cyt*c* is a soluble electron carrier between complex cytochrome bc_1 (cytbc_1) and cytochrome *c* oxidase (C*c*o) in the aerobic mitochondrial respiration. cytc_2 are found in the periplasmic space of nonsulfur purple photosynthetic bacteria, where they usually shuttle electrons from cytbc_1 to the photosynthetic reaction center (RC).[7,8] The relatively higher redox potential of cytc_2 is believed to be a direct consequence of its need to adaptation to photosynthetic ET. In fact, the E^0 of RCs is usually in the 450−500 mV range, while cytochrome *c* oxidase complexes, the electron acceptor in mitochondrial respiration, and therefore the RC counterpart for cyt*c* display significantly lower reduction potentials.[9,10]

Previous experimental[11−14] and theoretical[3,4,15,16] studies on cytochromes investigated the effects of structural features on E^0, such as the protein folding, the number and type of axial ligands, the presence of charged groups close to the heme, and its solvent exposure, but how can differences in reduction potential displayed by species with strikingly similar structures, as in the case of cyt*c* and cytc_2, be justified?

The elucidation of the molecular determinants to the quite distinct properties of prokaryote and eukaryote cytochromes has kept scientists busy for a long time.[3,4,8,9] The most recent papers on this issue followed a general change of perspective in the investigation of biomolecules, characterized by a strong interest for the dynamic properties of proteins and by the awareness that conformations differing from the most

Received: March 13, 2014
Accepted: April 11, 2014
Published: April 11, 2014

dx.doi.org/10.1021/jz5005208 | J. Phys. Chem. Lett. 2014, 5, 1534−1540

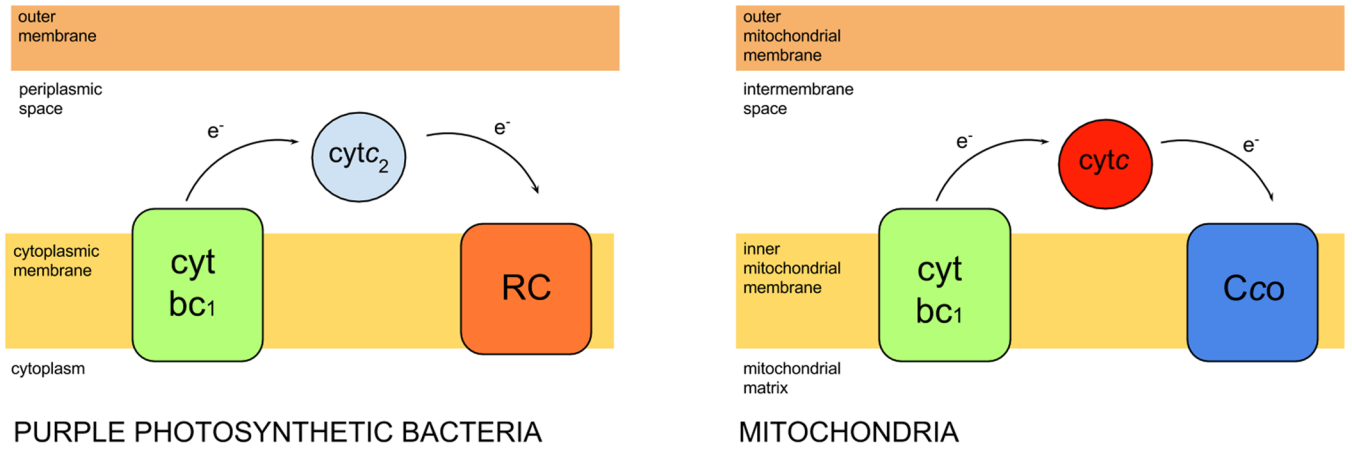

Figure 1. Schematic representation of the role and localization of soluble electron carriers cytc_2 and cyt*c* in photosynthetic bacteria and mitochondria, respectively.

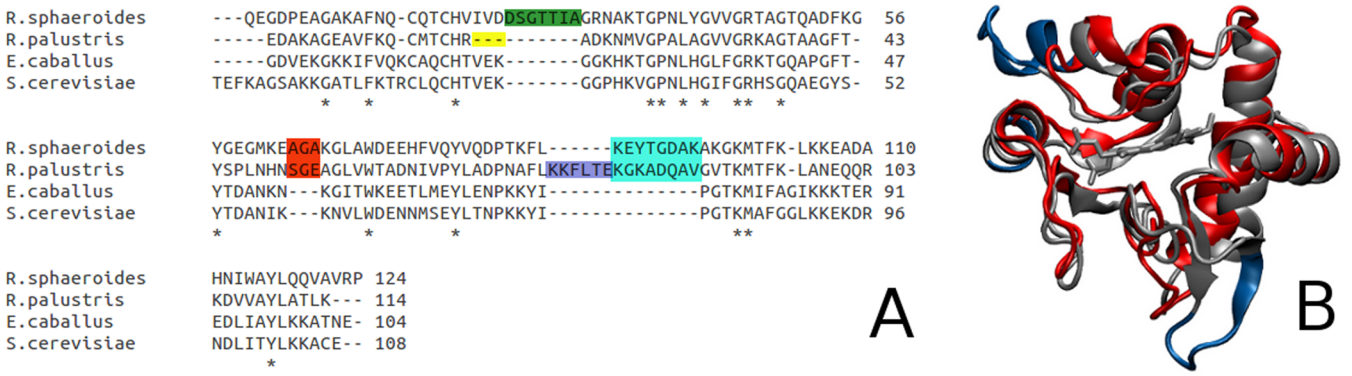

Figure 2. (A) Sequence alignment of the investigated cytochromes, obtained via Clustal Omega[20] and manually adjusted as suggested by Meyer et al.[21] Color coding of indels closely follows that of ref 21 to facilitate the comparison with previously reported sequence alignments between cytochromes. Conserved residues that are present in all four sequences are marked with an asterisk. (B) Superimposition of the 3-D structures of reduced horse heart cyt*c* (red, PDB code 1HRC) and *Rb. sphaeroides* cytc_2 (gray, while blue was used to highlight the structural elements of *Rb. sphaeroides* that are missing/different in horse heart cyt*c*; PDB code 1CXC). For the sake of clarity, only one heme group is shown. The image was produced with the VMD software.[22]

populated, time-averaged structure can be functionally extremely relevant.[17] The growing awareness that the somehow "static" structural properties obtained by crystal structures can not fully account for the physiological behavior of proteins[18,19] has led us to explore the dynamics of cytochromes with very similar structures but belonging to different families in the search for both common and singular aspects that would contribute to determine their reduction thermodynamics.

Here we compare the redox thermodynamic properties of mitochondrial cyt*c* and bacterial cytc_2, investigating two members of the first subfamily, namely, cyt*c* form baker's yeast (*S. cerevisiae*) and from horse heart (*E. caballus*), and two cytc_2 from nonsulfur purple photosynthetic bacteria *Rb. sphaeroides* and *Rps. palustris*. We started our investigation by comparing their amino acid sequences and 3-D structures. The sequences were aligned using the Clustal Omega web server.[20] The results provided by the server were manually adjusted following the work of Meyer et al.[21] to highlight the presence of insertions and deletions (indels) that were suggested to be significant from an evolutionary point of view. The final result of the alignment is reported in Figure 2A. The sequences of the two mitochondrial cyt*c* are rather close (63% identity). The two cytc_2 display higher sequence diversity, but one feature is common to both cytc_2 from *Rps. palustris* and *Rb. sphaeroides*, which is the most significant difference with the primary structures of mitochondrial cyt*c*: the presence of two insertions, 3- and 8-residues long, respectively, which were hypothesized to be involved in the peripheral interaction with the photosynthetic RC.[21] Still, the investigated cytochromes can be considered to be very closely related from a structural point of view,[9] as witnessed by the superimposition of 3-D structures of horse heart cyt*c* and *Rb. sphaeroides* cytc_2 (Figure 2B), highlighting the longer α-helix and loop right before the iron-coordinating methionine (Met80 in horse heart numbering) and the presence of two short regions of β-sheet in the longer N-terminal ω-loop of cytc_2 , at variance with a single β-sheet region in the corresponding loop of mitochondrial cyt*c*. The members of the two classes share a His,Met axial coordination of the iron atom of the heme, the latter being covalently bound to the polypeptidic matrix via the highly conserved CXXCH binding site near the N-terminus, and they both feature a globular fold. Moreover, independently of the net overall protein charge, both cytochrome families are characterized by the presence of a number of positively charged residues surrounding the solvent-exposed heme-edge, which are known to be crucial in the long-range electrostatic interaction with ET partners.[9] Inspection of the surroundings of the protein active sites, in terms of the presence of amino acids with charged side

dx.doi.org/10.1021/jz5005208 | *J. Phys. Chem. Lett.* 2014, 5, 1534−1540

chains in the vicinity of the metal ion, further proved the high structural homology between the mitochondrial and bacterial cytochromes and confirmed that the more positive E^0 values for the latter cannot be explained just on the basis of local electrostatic effects.

To estimate the reduction potentials, we first performed 110 ns long molecular dynamics (MD) simulations of the four cytochromes at 298 K and infinite dilution in both their reduced and oxidized ensemble. Several methods have been employed for the theoretical calculation of reduction potential of metalloproteins at different levels of the theory.[3,23−27] In our case, E^0 was calculated by applying the mixed quantum mechanics/molecular mechanics approach named perturbed matrix method (PMM)[28−33] to the MD simulations, closely paralleling the procedure used in our previous papers[34,35] (more details are provided afterward).

The (Helmholtz) free-energy change upon reduction, ΔA^0, that is related to the reduction potential via $E^0 = -\Delta A^0/F$ (where F is the Faraday constant) was calculated using the following equation

$$\Delta A^0 \cong \frac{-kT \ln\langle e^{-\beta\Delta\mathcal{U}}\rangle_{ox} + kT \ln\langle e^{\beta\Delta\mathcal{U}}\rangle_{red}}{2} \quad (1)$$

where $\Delta\mathcal{U}$ (i.e., the transition energy) is calculated as $\varepsilon_{red} - \varepsilon_{ox}$, with ε_{red} and ε_{ox} representing the perturbed ground-state electronic energy of the red (reduced) and ox (oxidized) chemical states of the redox center interacting with the environment, respectively.[35] ε_{red} and ε_{ox} are evaluated at each MD frame via the PMM approach, and the averaging is performed in either the reduced or oxidized ensemble, as indicated by the angle brackets subscript. The calculated E^0 are listed in Table 1, together with the associated ΔA^0 values.

Table 1. Experimental and Calculated Values of the Reduction Potential E^0 for the Investigated Cytochromes[a]

	family	E^0_{calc} (V)	E^0_{exp} (V)	ΔA^0_{calc} (kJ/mol)
horse heart (*E. caballus*)	cyt*c*	4.67	4.726	−450
yeast (*S. cerevisiae*)	cyt*c*	4.70	4.711	−453
Rps. palustris	cytc_2	4.78	4.808	−461
Rb. sphaeroides	cytc_2	4.77	4.774	−460

[a]Associated errors are ±0.020, ±0.002, and ±1.88 kJ/mol for E^0_{calc}, E^0_{exp}, and ΔA^0_{calc}, respectively. The standard error for the calculated properties was obtained by averaging the estimated standard errors of the four cytochromes. As the comparison of the experimental E^0 values with the calculated ones requires absolute reduction potentials, the IUPAC recommended 4.420 V value for the hydrogen semireaction[36,37] was added to the experimental E^0 extrapolated at zero ionic strength versus SHE.

Convergence for both terms in eq 1 was generally reached within ∼80 ns. Time convergence plots can be found in the Supporting Information (SI).

The reliability of our computational approach was assessed by comparing the calculated E^0 with the experimental values at 298 K extrapolated at infinite dilution, which are also listed in Table 1. Figure 3 displays the plot of calculated E^0 versus the corresponding experimental values. An extremely good agreement between the two data sets can be observed, proving that our approach could predict both the general trend of the E^0 (i.e., the relative reduction potentials) and yield an extremely satisfactory estimation of the absolute values. In fact, the bacterial cytc_2 and the mitochondrial cyt*c* are grouped into two

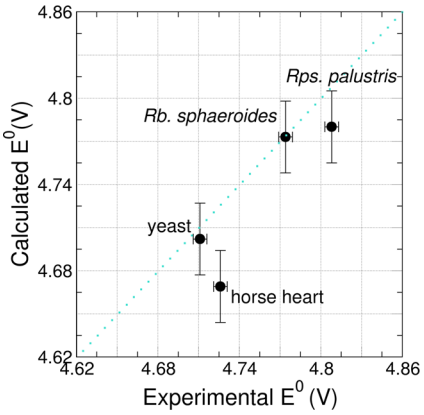

Figure 3. Calculated versus experimental E^0 values. The dashed turquoise line provides a guide for the eye, representing the ideal correspondence between theoretical and electrochemical data.

distinct subsets, with the latter having more negative potentials. These results provide a strong evidence of the predictive capability of our theoretical approach for redox thermodynamic properties of complex systems: while the prediction of the absolute E^0 is clearly dependent on the choice of the value for the hydrogen semireaction, the ability to reproduce $\Delta\Delta A^0$ as low as 8−10 kJ/mol is definitely a strong point of the present computational strategy. The test against experimental data allowed us to further use these simulations in our search for the reasons underlying the differences in reduction potentials between cyt*c* and cytc_2.

In a previous paper,[35] we derived a general theoretical model based on rigorous statistical mechanical relations, providing the thermodynamics of redox processes. The derivation was not based on the usual Gaussian approximation for the energy change associated with the redox process, thus resulting in a completely general model for describing redox reactions. One of the key points in our derivation was the existence of two distinct reorganization free energies, λ_{red} and λ_{ox}, corresponding to the relaxation free energy for the oxidized to reduced (ox → red) or reduced to oxidized (red → ox) state transitions, respectively. The reorganization free energies can be calculated as[35]

$$\lambda_{red} \cong \langle\Delta\mathcal{U}\rangle_{ox} - \Delta A^0 - kT \ln\frac{\sigma_{red}}{\sigma_{ox}} \quad (2)$$

$$\lambda_{ox} \cong -\langle\Delta\mathcal{U}\rangle_{red} + \Delta A^0 + kT \ln\frac{\sigma_{red}}{\sigma_{ox}} \quad (3)$$

where σ_{red} and σ_{ox} are the standard deviations of the corresponding transition energy distributions.

For the four cytochromes, we calculated λ_{red}, λ_{ox}, (see Table 2) and the corresponding mean values, $\lambda = (\lambda_{red} + \lambda_{ox})/2$, the latter being directly comparable to experimentally estimated reorganization free energies. For the two cyt*c*, we obtain $\lambda \approx 85$ kJ/mol (0.88 eV), which is in good agreement with the experimental estimation of λ for cytochromes *c* of 0.8 eV.[38] This good agreement serves as a further benchmark for the reliability of our calculations.

A relevant result of our derivation[35] was the possibility to explicitly relate the reduction free energy to the difference, $\Delta\lambda$, between the reorganization free energies λ_{red} and λ_{ox} ($\Delta\lambda = \lambda_{red} - \lambda_{ox}$)

dx.doi.org/10.1021/jz5005208 | J. Phys. Chem. Lett. 2014, 5, 1534−1540

Table 2. Redox Thermodynamic Properties As Obtained from the MD Simulations and PMM Calculations Performed for the Four Investigated Cytochromes[a]

	λ_{ox}	λ_{red}	$\Delta\lambda$	$\frac{\langle\Delta\mathcal{U}\rangle_{ox} + \langle\Delta\mathcal{U}\rangle_{red}}{2}$	$kT \ln \sigma_{red}/\sigma_{ox}$
horse heart	87	84	−3	−452.1	−0.2
yeast	83	87	4	−452.1	−0.3
Rps. palustris	68	93	25	−448.7	−0.1
Rb. sphaeroides	74	81	7	−457.4	−0.4

[a]All data are expressed in kJ/mol. Associated errors are ±2 kJ/mol for λ_{ox}, λ_{red}, and $\Delta\lambda$ and ±0.5 kJ/mol for $(\langle\Delta\mathcal{U}\rangle_{ox} + \langle\Delta\mathcal{U}\rangle_{red})/2$. The standard error for the calculated properties was obtained by averaging the estimated standard errors of the four cytochromes.

$$\Delta A^0 = \frac{\langle\Delta\mathcal{U}\rangle_{ox} + \langle\Delta\mathcal{U}\rangle_{red}}{2} - kT \ln \frac{\sigma_{red}}{\sigma_{ox}} - \frac{\Delta\lambda}{2} \quad (4)$$

The only approximations used to derive eq 4 are (i) that the vibrational partition functions of the reactants and products are virtually identical and (ii) that the transition energy fluctuations close to the transition energy probability maximum (i.e., close to the mean transition energy) is well-described by a quadratic behavior for both reactants and products.[35]

The dependency of the calculated reduction free energies of the four cytochromes on the corresponding variations in the reorganization free energies is displayed in Figure 4, which remarkably shows that within the noise the free energies of the four cytochromes are well-described by a linear behavior, corresponding (in eq 4) to the case in which

$$\frac{\langle\Delta\mathcal{U}\rangle_{ox} + \langle\Delta\mathcal{U}\rangle_{red}}{2} - kT \ln \frac{\sigma_{red}}{\sigma_{ox}}$$

is roughly constant for all investigated cytochromes, that is

$$\frac{\langle\Delta\mathcal{U}\rangle_{ox} + \langle\Delta\mathcal{U}\rangle_{red}}{2} - kT \ln \frac{\sigma_{red}}{\sigma_{ox}} \cong q_{cyt}$$

independently of the cytochrome type. Linear regression of the cytochromes free energies by using $\Delta A^0 = q_{cyt} - (\Delta\lambda/2)$, which corresponds to the pure linear behavior given by eq 4, provides $q_{cyt} = -452.3 \pm 0.5$ kJ/mol. (See Figure 4.) Note that the assumption of the simple linear behavior accurately describes the redox free energies, as clearly indicated by the high correlation coefficient ($r = 0.81$) of the regression. Therefore, it is reasonable to assume that all of the investigated cytochromes, although in completely diverse organisms and accomplishing different biological tasks, are rather similar for what concerns the first two transition energy moments (i.e., the mean and standard deviation), which determine the first two terms in eq 4, yielding a roughly constant contribution q_{cyt} to the total ΔA^0. The differences of the redox thermodynamics among the species are therefore essentially caused by rare fluctuations in the transition energy, resulting in a nonzero $\Delta\lambda$, inherent to a complex tail behavior of the transition energy distribution. Note that within the usual Gaussian approximation for the transition energy distribution $\Delta\lambda$ would be zero and hence all cytochromes' redox free energies would be virtually the same within the q_{cyt} noise. Because the reorganization energy λ is a rather complex quantity that is affected by the protein matrix, the solvent, and their mutual interaction,[23,39−41] it is unlikely that a single molecular descriptor can fully account for the differences in $\Delta\lambda$. Nevertheless, the accessibility of the solvent

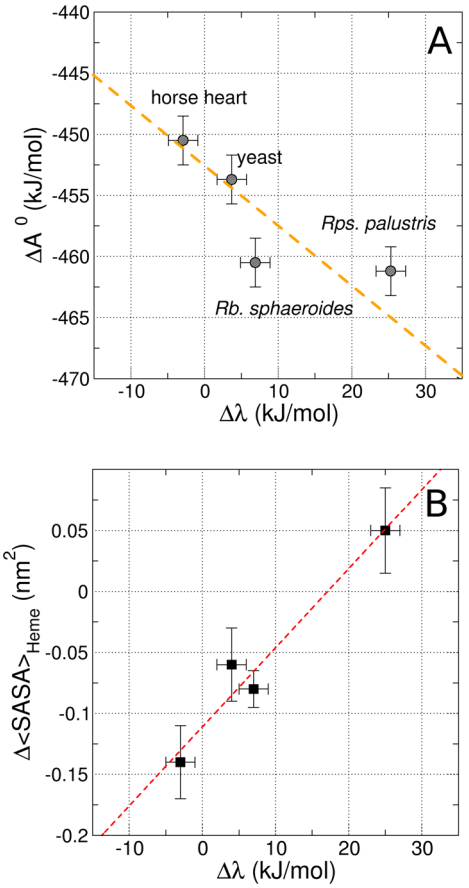

Figure 4. (A) Plot of calculated ΔA^0 versus calculated $\Delta\lambda$. The orange line represents a linear fit to the function $\Delta A^0 = q_{cyt} - (\Delta\lambda/2)$. (B) Plot of the calculated difference $\Delta\langle SASA\rangle_{Heme}$ versus calculated $\Delta\lambda$. The red line represents the linear regression between the four points, featuring a correlation coefficient $r = 0.97$.

to the heme was previously suggested as one of the main determinants to λ.[39,41] We therefore calculated the average value of the solvent accessible surface area (SASA) of the heme $\langle SASA\rangle_{Heme}$ in both the reduced and oxidized ensembles for all species and obtained the changes in the mean heme SASA upon reduction $\Delta\langle SASA\rangle_{Heme}$ as $\langle SASA\rangle_{Heme,red} - \langle SASA\rangle_{Heme,ox}$. Plotting $\Delta\langle SASA\rangle_{Heme}$ against the corresponding $\Delta\lambda$ values leads to a roughly linear correlation between the two quantities (see Figure 4B), thus suggesting that the different changes in the heme solvent accessibility upon reduction could be one of the determinants of the observed differences in $\Delta\lambda$.

Comparison of eq 4 with $\Delta A^0 = \Delta U^0 - T\Delta S^0$ suggests that also ΔU^0 and ΔS^0 are likely to be linear in $\Delta\lambda$, hence indicating that variations in $\Delta\lambda$ provide changes in the reduction entropy. Experimentally derived ΔS^0 obtained by means of electrochemical measurements, although not at null ionic strength, support this hypothesis: in fact, ΔS^0 for *Rps. palustris* and *Rb. sphaeroides* are −67 ± 6 and −69 ± 6 J mol^{-1} K^{-1}, respectively,[42] while mitochondrial cytc from horse heart and yeast exhibit more positive ΔS^0 values (−49 ± 4[43] and −44 ± 6[44] J mol^{-1} K^{-1}, respectively), providing a roughly linear relation with the corresponding $\Delta\lambda$ values (see Table 2).

The investigation of the factors affecting E^0 led us to collect evidence that the reduction potential of cytochromes can be regarded as the result of the sum of two terms: the first one is mainly dependent on the energy fluctuations within a limited

dx.doi.org/10.1021/jz5005208 | J. Phys. Chem. Lett. 2014, 5, 1534−1540

range around the mean transition energy; the second depends linearly on the difference of the reorganization free energies for the ox → red and for the red → ox relaxations, that is, on the $\Delta\lambda$. We found that the first term is similar for all cytochromes investigated and that the discrepancies in E^0 among the analyzed cytochromes can be ascribed to differences in $\Delta\lambda$. Moreover, this work serves as a solid benchmark for the PMM predicting capability of redox thermodynamics of heme-metalloproteins, which can be, in general, employed to investigate redox processes of any complex system, especially when dynamics aspects are likely to play a major role.

Molecular Dynamics Simulations. The MD simulations of the four cytochromes were performed using the GROMACS software package.[45] The starting coordinates for the MD simulations of cytc_2 for *Rb. sphaeroides* and *Rps. palustris* and for horse heart cyt*c* were taken from the corresponding crystal structures (PDB codes: 1CXC,[46] 1FJ0[47] and 1HRC,[48] respectively). For all the details concerning the simulation of yeast cytochrome *c*, please refer to ref.[34] Each protein was put at the center of a dodecahedron box large enough to contain ∼1.0 nm of water on all sides, modeled with the simple point charge (SPC)[49] model. The simulations were performed in the NVT ensemble at the experimental temperature of 298 K. The temperature was kept constant by the isokinetic temperature coupling.[50] The Gromos96 (53a6 version) force-field parameters[51] were adopted for the protein and the heme in its reduced form. The atomic partial charges for the oxidized heme and the missing parameters describing axial and covalent links between the protein and the heme were parametrized using quantum chemical calculations. (Details can be found in ref 34.) 110 ns long trajectories were run for both the reduced and oxidized forms of the four cytochromes. For the analysis, the first 10 ns of each simulation was removed. More details of the MD simulations can be found in the SI.

Perturbed Matrix Method. The main feature of the PMM[28−33] is that the portion of the system directly involved in the chemical reaction, hereafter termed as quantum center (QC), is treated explicitly at the electronic level, with the rest of the system described at a classical atomistic level exerting the electrostatic perturbation on the QC electronic states. Therefore, when performing PMM calculations, the first step is the choice of the QC. In the present work, the QC includes the atoms of the prosthetic group and those of the side chains of the axial ligands, that is, one histidine and one methionine. The second step is the extraction of a reference QC geometry for the evaluation of the unperturbed electronic eigenfunctions and related properties to be used in the PMM procedure. Here we chose as reference QC structure its most populated geometry along the reduced cyt *c* MD simulations (which is very closed to the corresponding geometry in the crystal structure). To avoid spurious effects on the quality of the calculated unperturbed wave functions, we refined the chosen QC structure by performing quantum-chemical energy minimization using the internal coordinates framework, keeping frozen the semiclassical degrees of freedom, that is, essentially dihedral and torsion angles. This QC reference structure is assumed to be representative of all possible QC structures, as obtained within the MD simulation. This assumption massively reduces the computational cost for the quantum-chemical calculations by allowing the use of single-structure quantum chemical calculations providing the unperturbed basis set and related properties. Such an approximation is typically rather accurate when the considered QC is rigid or semirigid, as in the present case, and hence no relevant deformations are accessible within the MD simulations. During step three, an orthonormal set of unperturbed (i.e., isolated in vacuo) electronic Hamiltonian ($\tilde{H}^0$) eigenfunctions (Φ_k^0) is evaluated on the QC structure of interest. The details of the quantum-chemical calculations performed on the isolated QC to obtain the unperturbed electronic energies and related properties are reported in the SI. Indicating with $\mathcal{V}$ and $\mathbf{E}$ the perturbing electric potential and field, respectively, exerted by the environment on the QC (typically obtained by the environment atomic charge distribution and evaluated in the QC center of mass), we may then (step four) construct for each QC environment configuration (as generated by explicit solvent MD simulation) the perturbed electronic Hamiltonian matrix ($\tilde{H}$) as follows

$$\tilde{H} \cong \tilde{H}^0 + \tilde{I} q_T \mathcal{V} + \tilde{Z}_1 + \Delta V \tilde{I} \tag{5}$$

$$[\tilde{Z}_1]_{k,k'} = -\mathbf{E}\cdot\langle \Phi_k^0 | \hat{\mu} | \Phi_{k'}^0 \rangle \tag{6}$$

q_T and $\hat{\mu}$ are the QC total charge and dipole operator, respectively, ΔV approximates all of the higher order terms as a simple short-range potential, $\tilde{I}$ is the identity matrix, and the angled brackets indicate integration over the electronic coordinates. ΔV is typically considered independent of the redox state and hence does not contribute to the transition energy (i.e., the energy change due to the redox-state transition). The diagonalization of $\tilde{H}$ provides a set of eigenvectors and eigenvalues representing the QC perturbed electronic eigenstates and energies (ε). The use of this procedure at each MD frame provides the instantaneous perturbed electronic eigenfunctions and energies, which in turn can be used to evaluate the reaction redox potential. For the purpose of calculating redox potentials for the present work, the quantity of interest is the perturbed electronic ground-state energy, which was calculated for both redox states of the QC, that is, Fe^{+2} and Fe^{+3}, providing ε_{red} and ε_{ox}, respectively.

Reduction Potentials. In the present paper, we consider the reduction potential for the $Fe^{+3} + e^- \rightarrow Fe^{+2}$ semireaction at 298 K and infinite dilution conditions in both the experimental and theoretical/computational evaluations. In the PMM/MD calculations, the (Helmholtz) free-energy change upon reduction (ΔA^0) was calculated using the following equation (ΔA^0 is related to the reduction potential via $E^0 = -\Delta A^0/F$)

$$\Delta A^0 \cong -k_B T \ln\langle e^{-\beta\Delta\mathcal{U}}\rangle_{ox} = k_B T \ln\langle e^{\beta\Delta\mathcal{U}}\rangle_{red} \tag{7}$$

In the above equation, $\Delta\mathcal{U} \cong \varepsilon_{red} - \varepsilon_{ox}$ and the averaging is performed in either the reduced or oxidized ensemble, as indicated by the angle brackets subscript. Although eq 7 is based on in principle an exact relation, given the sampling problems of finite-time simulations, the best estimate of the reduction free energy is obtained by averaging the values provided by the reduced and oxidized ensembles, see eq 1.[52]

Experimentally, reduction potential values at 298 K, constant pressure, and infinite dilution were taken from the literature,[34,53,54] except for the cytc_2 from *Rb. sphaeroides*, for which the E^0 at null ionic strength (corresponding to infinitely diluted reactants and products) was extrapolated by performing electrochemical measurements at different ionic strength values.

dx.doi.org/10.1021/jz5005208 | J. Phys. Chem. Lett. 2014, 5, 1534−1540

■ ASSOCIATED CONTENT

Supporting Information

Details of the computational procedures and on the electrochemical measurements. This material is available free of charge via the Internet at http://pubs.acs.org.

■ AUTHOR INFORMATION

Corresponding Author

*E-mail: carloaugusto.bortolotti@unimore.it.

Notes

The authors declare no competing financial interest.

■ ACKNOWLEDGMENTS

We acknowledge the CINECA award IsC11_PHOSPHO under the ISCRA initiative for the availability of high-performance computing resources and support. The research leading to these results has received funding from the European Union Seventh Framework Programme [FP7/2007-2013] under grant agreement no. 280772, project iONE-FP7.

■ REFERENCES

(1) Moore, G. R.; Pettigrew, G. W. *Cytochromes c: Evolutionary, Structural and Physicochemical Aspects*; Springer-Verlag: Berlin, 1990.

(2) Wilson, M. T.; Greenwood, C. In *Cytochrome c: A Multidisciplinary Approach*; Scott, R., Mauk, G., Eds.; University Science Books: Sausalito, CA, 1996.

(3) Mao, J.; Hauser, K.; Gunner, M. R. How Cytochromes with Different Folds Control Heme Redox Potentials. *Biochemistry* **2003**, *42*, 9829−9840.

(4) Zheng, Z.; Gunner, M. R. Analysis of the Electrochemistry of Hemes With E(m)s Spanning 800 mV. *Proteins* **2009**, *75*, 719−734.

(5) Bendall, D. *Protein Electron Transfer*; BIOS Scientific Publisher, Ltd: Oxford, U.K., 1996.

(6) Meyer, T. E.; Cusanovich, M. a.; Kamen, M. D. Evidence Against Use of Bacterial Amino Acid Sequence Data for Construction of All-Inclusive Phylogenetic Trees. *Proc. Natl. Acad. Sci. U.S.A.* **1986**, *83*, 217−220.

(7) Moser, C. C.; Dutton, P. L. Cytochrome c and c2 Binding Dynamics and Electron Transfer with Photosynthetic Reaction Center Protein and Other Integral Membrane Redox Proteins. *Biochemistry* **1988**, *27*, 2450−2461.

(8) Axelrod, H. L.; Okamura, M. Y. The Structure and Function of the Cytochrome c2: Reaction Center Electron Transfer Complex from Rhodobacter sphaeroides. *Photosynth. Res.* **2005**, *85*, 101−114.

(9) Meyer, T. E.; Cusanovich, M. A. Discovery and Characterization of Electron Transfer Proteins in the Photosynthetic Bacteria. *Photosynth. Res.* **2003**, *76*, 111−126.

(10) Wachveitl, J.; Farchaus, J.; Das, R.; Lutz, M.; Robert, B.; Matitoli, T. Structure, Spectroscopic, and Redox Properties of Rhodobacter sphaeroides Reaction Centers Bearing Point Mutations Near the Primary Electron Donor. *Biochemistry* **1993**, *32*, 12875−12886.

(11) Mauk, A.; Moore, G. Control of Metalloprotein Redox Potentials: What Does Site-Directed Mutagenesis of Hemoproteins Tell Us. *J. Biol. Inorg. Chem.* **1997**, *2*, 119−125.

(12) Tezcan, F.; Winkler, J.; Gray, H. Effects of Ligation and Folding on Reduction Potentials of Heme Proteins. *J. Am. Chem. Soc.* **1998**, *120*, 13383−13388.

(13) Worrall, J. A. R.; Schlarb-Ridley, B. G.; Reda, T.; Marcaida, M. J.; Moorlen, R. J.; Wastl, J.; Hirst, J.; Bendall, D. S.; Luisi, B. F.; Howe, C. J. Modulation of Heme Redox Potential in the Cytochrome c6 Family. *J. Am. Chem. Soc.* **2007**, *129*, 9468−9475.

(14) Osyczka, A.; Dutton, P. L.; Moser, C. C.; Darrouzet, E.; Daldal, F. Controlling the Functionality of Cytochrome c(1) Redox Potentials in the Rhodobacter capsulatus bc(1) Complex through Disulfide Anchoring of a Loop and a Beta-Branched Amino Acid Near the Heme-Ligating Methionine. *Biochemistry* **2001**, *40*, 14547−14556.

(15) Ishikita, H.; Loll, B.; Biesiadka, J.; Saenger, W.; Knapp, W. E. Redox Potentials of Chlorophylls in Photosystem II Reaction Center. *Biochemistry* **2005**, *44*, 4118−4124.

(16) Sham, Y.; Chu, Z.; Warshel, A. Consistent Calculations of pKa's of Ionizable Residues in Proteins: Semi-Microscopic and Microscopic Approaches. *J. Phys. Chem.* **1997**, *101*, 4458−4472.

(17) Cheng, G.; Wysocki, V. H.; Cusanovich, M. a. Local Stability of Rhodobacter capsulatus Cytochrome c2 Probed by Solution Phase Hydrogen/Deuterium Exchange and Mass Spectrometry. *J. Am. Soc. Mass Spectrom.* **2006**, *17*, 1518−1525.

(18) Henzler-Wildman, K.; Kern, D. Dynamic Personalities of Proteins. *Nature* **2007**, *450*, 964−972.

(19) Gaspari, Z.; Perczel, A. In *Annu. Rep. NMR Spectrosc.*; Webb, G. A., Ed.; Academic Press: Burlington, MA, 2010; pp 35−75.

(20) Sievers, F.; Wilm, A.; Dineen, D.; Gibson, T. J.; Karplus, K.; Li, W.; Lopez, R.; McWilliam, H.; Remmert, M.; Soeding, J.; Thompson, J. D.; Higgins, D. G. Fast, Scalable Generation of High-Quality Protein Multiple Sequence Alignments Using Clustal Omega. *Mol. Syst. Biol.* **2010**, *7*, 539.

(21) Meyer, T.; Van Driessche, G.; Ambler, R.; Kyndt, J.; Devreese, B.; Van Beeumen, J.; Cusanovich, M. Evidence from the Structure and Function of cytochromes c(2) that Nonsulfur Purple Bacterial Photosynthesis Followed the Evolution of Oxygen Respiration. *Arch. Microbiol.* **2010**, *192*, 855−865.

(22) Humphrey, W.; Dalke, A.; Schulten, K. VMD − Visual Molecular Dynamics. *J. Mol. Graphics* **1996**, *14*, 33−38.

(23) Cascella, M.; Magistrato, A.; Tavernelli, I.; Carloni, P.; Rothlisberger, U. Role of Protein Frame and Solvent for the Redox Properties of Azurin from Pseudomonas aeruginosa. *Proc. Natl. Acad. Sci. U.S.A.* **2006**, *103*, 19641−19646.

(24) Blumberger, J. Free Energies for Biological Electron Transfer from QM/MM Calculation: Method, Application and Critical Assessment. *Phys. Chem. Chem. Phys.* **2008**, *10*, 5651−5667.

(25) Breuer, M.; Zarzycki, P.; Blumberger, J.; Rosso, K. M. Thermodynamics of Electron Flow in the Bacterial Deca-Heme Cytochrome MtrF. *J. Am. Chem. Soc.* **2012**, *134*, 9868−9871.

(26) Perrin, B. S., Jr.; Niu, S.; Ichiye, T. Calculating Standard Reduction Potentials of [4Fe-4S] Proteins. *J. Comput. Chem.* **2013**, *34*, 576−582.

(27) Voigt, P.; Knapp, E. Tuning Heme Redox Potentials in the Cytochrome c Subunit of Photosynthetic Reaction Centers. *J. Biol. Chem.* **2003**, *278*, 1993−2001.

(28) Aschi, M.; Spezia, R.; Di Nola, A.; Amadei, A. A First Principles Method to Model Perturbed Electronic Wavefunctions: the Effect of an External Electric Field. *Chem. Phys. Lett.* **2001**, *344*, 374−380.

(29) Amadei, A.; D'Alessandro, M.; Aschi, M. Statistical Mechanical Modeling of Chemical Reactions in Complex Systems: the Reaction Free Energy Surface. *J. Phys. Chem. B* **2004**, *108*, 16250−16254.

(30) Aschi, M.; D'Abramo, M.; Ramondo, F.; Daidone, I.; D'Alessandro, M.; Di Nola, A.; Amadei, A. Theoretical Modeling of Chemical Reactions in Complex Environments: the Intramolecular Proton Transfer in Aqueous Malonaldehyde. *J. Phys. Org. Chem.* **2006**, *19*, 518−530.

(31) Zazza, C.; Amadei, A.; Palma, A.; Sanna, N.; Tatoli, S.; Aschi, M. Theoretical Modelling of Enzyme Reactions: the Thermodynamics of Formation of Compound 0 in Horseradish Peroxidase. *J. Phys. Chem. B* **2008**, *112*, 3184−3192.

(32) Daidone, I.; Aschi, M.; Zanetti-Polzi, L.; Nola, A. D.; Amadei, A. On the Origin of IR Spectral Changes upon Protein Folding. *Chem. Phys. Lett.* **2010**, *488*, 213−218.

(33) Amadei, A.; Daidone, I.; Nola, A. D.; Aschi, M. Theoretical-Computational Modelling of Infrared Spectra in Peptides and Proteins: a New Frontier for Combined Theoretical-Experimental Investigations. *Curr. Opin. Struc. Biol.* **2010**, *20*, 155−161.

(34) Bortolotti, C. A.; Amadei, A.; Aschi, M.; Borsari, M.; Corni, S.; Sola, M.; Daidone, I. The Reversible Opening of Water Channels in

Cytochrome c Modulates the Heme Iron Reduction Potential. *J. Am. Chem. Soc.* **2012**, *134*, 13670−13678.
(35) Amadei, A.; Daidone, I.; Bortolotti, C. A. A General Statistical Mechanical Approach for Modeling Redox Thermodynamics: the Reaction and Reorganization free energies. *RSC Adv.* **2013**, *3*, 19657−19665.
(36) Fawcett, W. The Ionic Work Function and its Role in Estimating Absolute Electrode Potentials. *Langmuir* **2008**, *24*, 9868−9875.
(37) Isse, A.; Gennaro, A. Absolute Potential of the Standard Hydrogen Electrode and the Problem of Interconversion of Potentials in Different Solvents. *J. Phys. Chem. B* **2010**, *114*, 7894−7899.
(38) Khoshtariya, D. E.; Wei, J.; Liu, H.; Yue, H.; Waldeck, D. H. Charge-Transfer Mechanism for Cytochrome. *J. Am. Chem. Soc.* **2003**, *125*, 7704−7714.
(39) Bortolotti, C. A.; Siwko, M. E.; Castellini, E.; Ranieri, A.; Sola, M.; Corni, S. The Reorganization Energy in Cytochrome c is Controlled by the Accessibility of the Heme to the Solvent. *J. Phys. Chem. Lett.* **2011**, *2*, 1761−1765.
(40) Paltrinieri, L.; Borsari, M.; Ranieri, A.; Battistuzzi, G.; Corni, S.; Bortolotti, C. A. The Active Site Loop Modulates the Reorganization Energy of Blue Copper Proteins by Controlling the Dynamic Interplay with Solvent. *J. Phys. Chem. Lett.* **2013**, *4*, 710−715.
(41) Tipmanee, V.; Oberhofer, H.; Park, M.; Kim, K. S.; Blumberger, J. Prediction of Reorganization Free Energies for Biological Electron Transfer: a Comparative Study of Ru-Modified Cytochromes and a 4-Helix Bundle Protein. *J. Am. Chem. Soc.* **2010**, *132*, 17032−17040.
(42) Battistuzzi, G.; Borsari, M.; Sola, M.; Francia, F. Redox Thermodynamics of the Native and Alkaline Form of Eukaryotic and Bacterial Class I Cytochromes c. *Biochemistry* **1997**, *36*, 16247−16258.
(43) Taniguchi, I.; Iskei, M.; Eto, T.; Toyosawa, K.; Yamaguchi, H.; Yasukouchi, K. The Effect of pH on the Temperature Dependence of the Redox Potential of Horse Heart Cytochrome c at a Bis(4-pyridil)disulfide-Modified Gold electrode. *Bioelectrochem. Bioenerg.* **1984**, *13*, 373−383.
(44) Bortolotti, C.; Battistuzzi, G.; Borsari, M.; Facci, P.; Ranieri, A.; Sola, M. The Redox Chemistry of the Covalently Immobilized Native and Low-pH Forms of Yeast Iso-1-Cytochrome c. *J. Am. Chem. Soc.* **2006**, *128*, 5444−5451.
(45) Berendsen, H. J. C.; van der Spoel, D.; van Drunen, R. ROMACS: A Message-Passing Parallel Molecular Dynamics Implementation. *Comput. Phys. Commun.* **1995**, *95*, 43−56.
(46) Axelrod, H.; Feher, G.; Allen, J.; Chirino, A.; Day, M.; Hsu, B.; Rees, D. Crystallization and X-Ray Structure Determination of Cytochrome c2 from Rhodobacter sphaeroides in Three Crystal Forms. *Acta Crystallogr., Sect. D: Biol. Crystallogr.* **1994**, *50*, 596−602.
(47) Geremia, S.; Garau, G.; Vaccari, L.; Sgarra, R.; Viezzoli, M.; Calligaris, M.; Randaccio, L. Cleavage of the Iron-Methionine Bond in c-type Cytochromes: Crystal Structure of Oxidized and Reduced Cytochrome c(2) from Rhodopseudomonas palustris and its ammonia Complex. *Protein Sci.* **2002**, *11*, 6−17.
(48) Bushnell, G.; Louie, G.; Brayer, G. D. High-resolution Three-Dimensional Structure of Horse Heart Cytochrome c. *J. Mol. Biol.* **1990**, *214*, 585−595.
(49) Berendsen, H. J. C.; Grigera, J. R.; Straatsma, T. P. The Missing Term in Effective Pair Potentials. *J. Phys. Chem.* **1987**, *91*, 6269−6271.
(50) Brown, D.; Clarke, J. H. R. A Comparison of Constant Energy, Constant Temperature, and Constant Pressure Ensembles in Molecular Dynamics Simulations of Atomic Liquids. *Mol. Phys.* **1984**, *51*, 1243−1252.
(51) van Gunsteren, W. F.; Billeter, S. R.; Eising, A. A.; Hünenberger, P. H.; Krüger, P.; Mark, A. E.; Scott, W. R. P.; Tironi, I. G. *Biomolecular Simulation: The GROMOS96 Manual and User Guide*; Hochschulverlag AG an der ETH Zürich: Zürich, 1996.
(52) Muegge, I.; Qi, P. X.; Wand, J.; Chu, Z. T.; Warshel, A. The Reorganization Energy of Cytochrome c Revisited. *J. Phys. Chem. B* **1997**, *101*, 825−836.
(53) Battistuzzi, G.; Borsari, M.; Dallari, D.; Lancellotti, I.; Sola, M. Anion Binding to Mitochondria1 Cytochromes c Studied Through Electrochemistry. Effects of the Neutralization of Surface Charges on the Redox Potential. *Eur. J. Biochem.* **1996**, *214*, 208−214.
(54) Battistuzzi, G.; Borsari, M.; Dallari, D.; Ferretti, S.; Sola, M. Cyclic Voltammetry and 1H-NMR of Rhodopseudomonas palustris Cytochrome c2. Probing Surface Charges through Anion-Binding Studies. *Eur. J. Biochem.* **1995**, *339*, 335−339.